*Progress In Electromagnetics Research C, Vol. 16, 85–98, 2010*

# BIT ERROR RATE REDUCTION FOR MULTIUSERS BY SMART UWB ANTENNA ARRAY

**S.-H. Liao, M.-H. Ho, and C.-C. Chiu**

Department of Electrical Engineering
Tamkang University
Tamsui, Taiwan, R.O.C.

**Abstract**—In this paper, a new ultra wideband circular antenna array (UCAA) combining genetic algorithm (GA) to minimize the bit error rate (BER) is proposed. The ultra wideband (UWB) impulse responses of the indoor channel for any transmitter-receiver location are computed by SBR/Image techniques, inverse fast Fourier transform and Hermitian processing. By using the impulse response of multipath channel, the BER performance of the binary pulse amplitude modulation (B-PAM) impulse radio (IR) UWB system with circular antenna array can be calculated. Based on the topography of the antenna and the BER formula, the array pattern synthesis problem can be reformulated into an optimization problem and solved by the genetic algorithm. The novelties of our approach is not only choosing BER as the object function instead of sidelobe level of the antenna pattern, but also considering the antenna feed length effect of each array element. The strong point of the genetic algorithm is that, it can find out the solution even if the performance index cannot be formulated by simple equations. Simulation results show that the synthesized antenna array pattern is effective to focus maximum gain to the multiusers.

## 1. INTRODUCTION

Ultra wideband (UWB) technology is an ideal candidate for a low power, low cost, high data rate, and short range wireless communication systems. According to the Federal Communication Commission (FCC), UWB signal is defined as a signal having fractional bandwidth greater than 20% of the center frequency [1]. Ultra wide bandwidth of the system causes antenna design to be a new challenge [2–5].

*Received 7 July 2010, Accepted 2 September 2010, Scheduled 14 September 2010*
Corresponding author: C.-C. Chiu (chiu@ee.tku.edu.tw).

Smart antennas employ arrays of antenna elements and can integrate multiple antenna elements with a signal processing. These smart antennas combine the signals from multiple antennas in a way that mitigate multipath fading and maximize the output signal-to-noise ratio. It can dramatically increase the performance of a communication system. The smart antenna technology in wireless communication can apply to the receiver [6, 7] and the transmitter [8, 9].

In the past, most papers apply genetic algorithms for searching the minimum sidelobe level of the antenna [10]. In [11], desired phase weights determined by the scan angle and array geometry, the amplitude weights of elements are optimized by differential evolution algorithm to drive down the side-lobes. However, this pattern cannot guarantee to obtain the minimum BER. Thus, we control the feed length of the array element.

When synthesizing the antenna array pattern to minimize the BER, the excitation problem is reformulated as optimization problem and the constraint conditions are often highly nonlinear and non-differentiable. Thus, we use the genetic algorithm to regulate the antenna feed length of each array element to minimize the BER. of each array element to minimize the BER.

In this paper, a smart circular transmitting antenna array is proposed at the transmitter to minimize the BER in UWB communication systems. Since, the UWB communication system spans a wide bandwidth in the frequency domain. Adjusting the same excitation phase delay of the UWB antenna for different frequencies is difficult. The genetic algorithm is used to regulate the antenna feed length of each array element to minimize the BER of the communication system. We regulate the amplitude and feed length of each array element to get a optimal radiation pattern which can minimize the BER. The remaining sections of this paper are organized as follows: Section 2 briefly explains the formulation of the problem which include antenna pattern, channel modeling and the BER calculation. Section 3 describes the genetic algorithm. The propagation modeling and numerical results are then presented in Section 4 and conclusion is made in Section 5.

## 2. SYSTEM DESCRIPTION

### 2.1. Circular Array Pattern

We consider a circular array of eight UWB printed dipole antennas, as shown in Fig. 1. $\ell_n$ is feed length of the $n$-th array element. Each element is uniformly distributed on a circle of radius $\Gamma$. Each

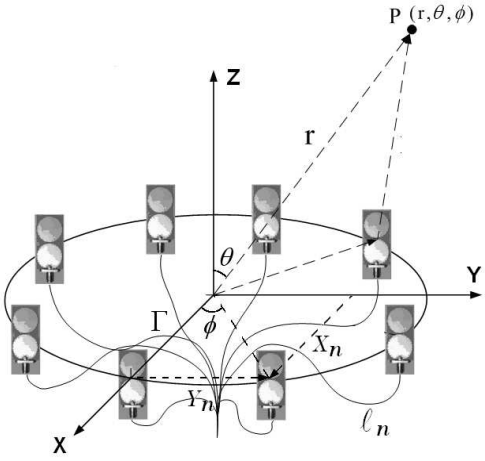


**Figure 1.** Geometry of a circular antenna of eight UWB printed dipole antennas.

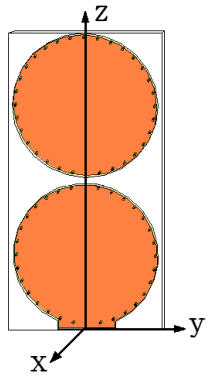


**Figure 2.** A UWB printed dipole antenna with circular arms.

element, as shown in Fig. 2, is the UWB printed dipole antenna with circular arms, which has been designed in [12, 13]. The radiation pattern between 3 GHz and 6 GHz is omnidirectional in the azimuth plane, which is interesting for communications between objects having undefined position in relation to each other. According to this advantage, we use this kind of antenna for circular array element. The array factor of this circular antenna array can be written as

$$AF(\theta,\phi,f)=\sum_{n=1}^{N_T-1} F_n \exp[-j\,(K\cdot X_n \sin\theta\cos\phi+K\cdot Y_n \sin\theta\sin\phi+\psi_n)] \tag{1}$$

where $\theta$ and $\phi$ are the spherical coordinate angles from the origin to the viewpoint in the elevation plane and azimuth plane. $f$ is the frequency of a sinusoidal wave. $N_T$ is the element number. $F_n$ and $\psi_n$ is the amplitude and phase delay of the excitation current for the $n$-th element respectively. $K = 2\pi/\lambda$ is the wavenumber, where $\lambda$ is the wavelength of the sinusoidal wave. $X_n$ and $Y_n$ are $x$-coordinate and $y$-coordinate positions of the $n$-th array element respectively. Thus the total radiation vector can be expressed as

$$\vec{N}(\theta,\phi,f) = AF(\theta,\phi,f)\cdot\vec{N}_e(\theta,\phi,f) \tag{2}$$

where $\vec{N}_e(\theta,\phi,f)$ is the radiation vector of individual element which can be obtained by the HFSS software based on the finite element method [14].

## 2.2. UWB Channel Modeling

The channel impulse response variations are significant for different types of antennas [15, 16], since the UWB communication spans a wide bandwidth in the frequency domain. We use the SBR/Image technique to calculate the channel impulse response which includes angular characteristics of radiation patterns and the variation between different frequencies of wave propagation.

SBR/Image techniques are good techniques to calculate channel frequency response for wireless communication [17, 18]. The SBR/Image technique conceptually assumes that many triangular ray tubes (not rays) are shot from a transmitter. Here, the triangular ray tubes whose vertexes are on a sphere are determined by the following method. First, we construct an icosahedron which is made of 20 identical equilateral triangles. Then, each triangle of the icosahedron is tessellated into a lot of smaller equilateral triangles. Finally, these small triangles are projected on to the sphere and each ray tube whose vertexes are determined by the small equilateral triangle is constructed. Then each ray tube will bounce and penetrate in the environments. If the receiver falls within the reflected ray tube, the contribution of the ray tube to the receiver can be attributed to an equivalent source (image). Using these images and received fields, the channel frequency response can be obtained as following

$$H(f) = \sum_{i=1}^{N_P} a_i(f) e^{j\theta_i(f)} \tag{3}$$

where $f$ is the frequency of sinusoidal wave, $i$ is the path index, $\theta_i$ is the $i$-th phase shift, $a_i$ is the $i$-th receiving magnitude which depends on the radiation vector of the transmitting and receiving antenna in (2). Note that the receiving antenna in our simulation is a omnidirectional UWB dipole antenna. On the other hand, the transmitter is the UWB circular antenna array (UCAA) which has been described in above section. The channel frequency response of UWB can be calculated by Equation (3) in the frequency range of UWB.

The frequency response is transformed to the time domain by using the inverse fast Fourier transform with the Hermitian signal processing [19]. Therefore the time domain impulse response of the equivalent baseband can be written as follows:

$$h_b(t) = \sum_{m=1}^{M_T} \alpha_m \delta(t - \tau_m) \tag{4}$$

where $M_T$ is the number of paths. $\alpha_m$ and $\tau_m$ are the channel gain and time delay for the $m$-th path respectively.

### 2.3. Formulation of BER

The entire link can be described in terms of the block diagram in Fig. 3. It shows the B-PAM UWB modulator, equivalent baseband impulse response $h_b(t)$ which includes the effect of the circular antenna array, B-PAM demodulator (a correlation receiver) and feed length controller (regulated by the GA to minimize BER).

As shown in Fig. 3, {b} is the input binary data stream and $\{\hat{b}\}$ is the output binary data stream after demodulator and decision device. When the binary data stream {b} passing through the B-PAM modulator, the transmitted UWB pulse stream is expressed as follows:

$$x(t) = \sum_{n=0}^{\infty} p(t - nT_d)d_n \tag{5}$$

where $E_t$ is the average transmitted energy and $p(t)$ is the transmitted waveform. $d_n \in \{\pm 1\}$ is a B-PAM symbol which corresponds to $\{b_n\}$ and is assumed to be independent identically distributed (i.i.d.). $T_d$ is the duration of the transmitting signal. The transmitted waveform $p(t)$ is the Gaussian waveform with ultra-short duration $T_p$ at the nanosecond scale. Note that $T_d$ is the duration of the transmitting signal and $T_p$ is the pulse duration. The value of $T_d$ is usually much larger than that of $T_p$. The Gaussian waveform $p(t)$ can be described

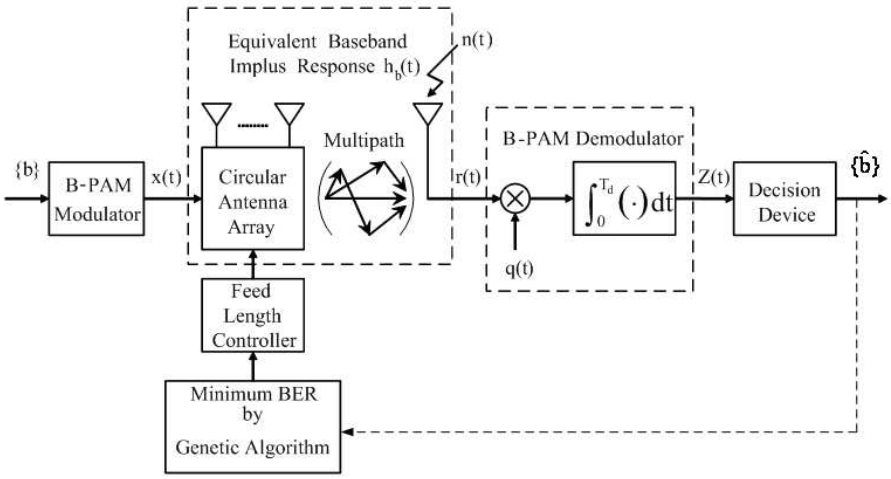


**Figure 3.** Block diagram of the simulated system.

by the following expression:

$$p(t) = \frac{1}{\sqrt{2\pi}\sigma} e^{\frac{-t^2}{2\sigma^2}} \tag{6}$$

where $t$ and $\sigma$ are time and standard deviation of the Gaussian wave, respectively. The average transmit energy symbol $E_t$ can be expressed as

$$E_t = \int_0^{T_d} p^2(t)dt \tag{7}$$

The received signal $r(t)$ can be expressed as follows:

$$r(t) = [x(t) \otimes h_b(t)] + n(t) \tag{8}$$

where $x(t)$ is the transmitted signal and $h_b(t)$ is the impulse response of the equivalent baseband, $n(t)$ is the white Gaussian noise with zero mean and variance $N_0/2$. The correlation receiver samples the received signal at the symbol rate and correlates them with suitably delayed references given by

$$q(t) = p[t - \tau_1 - (n-1)T_d] \tag{9}$$

where $\tau_1$ is the delay time of the first wave. The output of the correlator at $t = nT_d$.

$$\begin{aligned} Z(n) \;=\; & \int_{(n-1)T_d}^{nT_d} \left\{ \left[ \sum_{i=0}^{\infty} p(t - iT_d)d_i \right] \otimes h_b(t) \right\} \cdot q(t)dt \\ & + \int_{(n-1)T_d}^{nT_d} n(t)q(t)dt \quad = V(n) + \eta(n) \end{aligned} \tag{10}$$

It can be shown that the noise components $\eta(n)$ of (10) are uncorrelated Gaussian random variables with zero mean. The variance of the output noise $\eta$ is

$$\sigma^2 = \frac{N_0}{2} E_t \tag{11}$$

The conditional error probability of the $n$-th bit is thus expressed by:

$$P_e \left[ Z(n) | \vec{d} \right] = \frac{1}{2} erfc \left[ \frac{V(n)}{\sqrt{2}\sigma} \cdot (d_n) \right] \tag{12}$$

where $erfc(x) = \frac{2}{\sqrt{\pi}} \int_x^{\infty} e^{-y^2} dy$ is the complementary error function and $\{\vec{d}\} = \{d_0, d_1, \ldots d_n\}$ is the polar binary sequence. Note that the average BER for B-PAM impulse radio UWB system can be expressed as [20]

$$BER = \sum_{i=1}^{2^n} P\left(\vec{d}\right) \cdot \frac{1}{2} erfc \left[ \frac{V(i)}{\sqrt{2}\sigma} \cdot (d_n) \right] \tag{13}$$

## 3. GENETIC ALGORITHM

Genetic algorithms are the global numerical optimization methods based on genetic recombination and evaluation in nature [21, 22]. They use the iterative optimization procedures, which start with a randomly selected population of potential solutions. Then gradually evolve toward a better solution through the application of the genetic operators. Genetic algorithms typically operate on a discretized and coded representation of the parameters rather than on the parameters themselves. These representations are often considered to be "chromosomes", while the individual element, which constitutes chromosomes, is the "gene". Simple but often very effective chromosome representations for optimization problem involving several continuous parameters can be obtained through the juxtaposition of discretized binary representations of the individual parameter.

When analyzing the circular antenna array, the feed length of each array element provides the phase delay of excitation current which varies with different frequencies. The relationship between $n$-th antenna feed length $\ell_n$ and the excitation current phase delay $\psi_n$ can be expressed as follows:

$$\psi_n = \frac{2\pi}{\lambda}\ell_n \tag{14}$$

where $\lambda$ is the wavelength. Thus, we regulate the antenna feed length of each array element to get a optimal radiation pattern which can minimize the BER. The feed length of each array element can be decoded by the following equation:

$$\ell_n = Q_{\min} + \frac{Q_{\max} - Q_{\min}}{2^M - 1} \sum_{i=0}^{M-1} b_i^{\ell_n} 2^i \tag{15}$$

where $b_0^{\ell_n}, b_1^{\ell_n}, \ldots, b_{M-1}^{\ell_n}$ (genes) are M-bit strings of the binary representation of $\ell_n$. The $Q_{\min}$ and $Q_{\max}$ are the minimum and the maximum values admissible for $\ell_n$, respectively. In practical cases, $Q_{\min}$ and $Q_{\max}$ can be determined by the prior knowledge of the objects. Therefore, we set the $Q_{\min} = 0.0\,\text{cm}$ and $Q_{\max} = 10.0\,\text{cm}$ which is according to the minimum frequency 3 GHz. Then the unknown coefficients in (15) are described by a $N \times M$ bit string (chromosome). The genetic algorithm starts with a population containing a total of $N_p$ candidates (i.e., $N_p$ is the population size). Each candidate is described by a chromosome. Then the initial population can simply be created by taking $N_p$ random chromosomes. GA iteratively generates a new population, which is derived from the previous population through the application of the reproduction, crossover, and mutation operators.

The genetic algorithm is used to maximize the following fitness function ($FF$):

$$FF = \left\{ \sum_{i=1}^{2^n} P\left(\vec{d}\right) \cdot \frac{1}{2} erfc\left[ \frac{V(i)}{\sqrt{2}\sigma} \cdot (d_n) \right] \right\}^{-1} \tag{16}$$

where $FF$ is the inverse of the average BER for B-PAM IR UWB system. Through repeated applications of reproduction, crossover, and mutation operators, the initial population is transformed into a new population in an iterative manner. New populations will contain increasingly better chromosomes and will eventually converge to an optimal population that consists of the optimal chromosomes. In our simulation, when the fitness function is bigger than the threshold value or GA does not find a better individual within 300 successive generations. The genetic algorithm will be terminated and a solution is then obtained.

## 4. NUMERICAL RESULTS

A realistic environment was investigated. It consists of a living room with dimensions 10 m × 10 m × 3 m, housing one metallic cupboard and three wooden bookcases. Both of the cupboard and bookcase are 2 meter in height. The plan view of the simulated environment is shown in Fig. 4. Tx and Rx1, Rx2, Rx3 antennas were all mounted

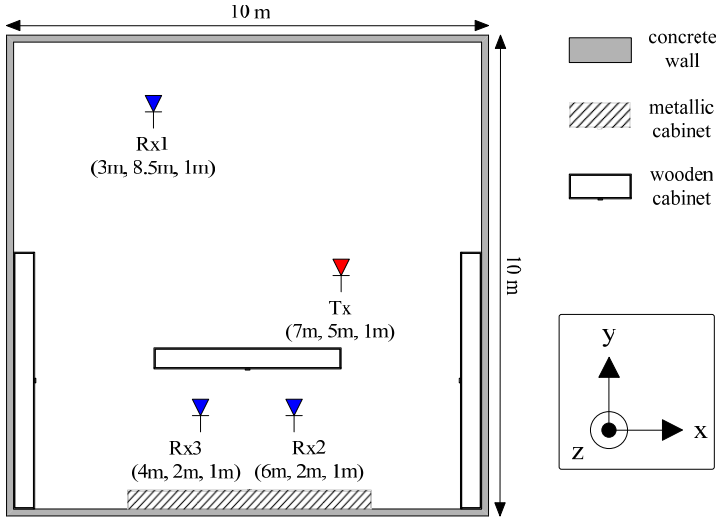


**Figure 4.** A plan view of the simulated environment.

1 meter above the floor. The transmitter Tx position is (7 m, 5 m, 1 m). We simulated two scenarios with different Rx positions. SBR/Image techniques combined antenna radiation pattern is used to calculate the UWB channel impulse response for each location of the receiver.

The frequency range of the UWB channel is simulated from 3 GHz to 6 GHz since the array element has the omnidirectional characteristic in this frequency range [12]. The specifications of the antenna and GA are set as below: The searching ranges of excitation voltage and feed Length are $0 \sim 1$ volt and $0 \sim 10$ cm, respectively. Then the unknown coefficients in (15) are described by a 10 bit string (chromosome). The parameter of the GA is set as below: The probability of crossover and mutation are set to 0.5 and 0.02 respectively. The population size set to 200.

Three kinds of transmitting antennas are used to in this simulation scenario: (a) Only one UWB printed dipole antenna (OUA). (b) A circular array of eight UWB printed Dipole antenna, each element antenna has the same feed Length without GA regulating (UCAA). (c) A circular array of eight UWB printed dipole antenna, each element antenna feed length was regulated by GA (UCAA-GA).

There are two receivers in Scenario I: one is a line-of-sight path at the Rx1 (3 m, 8.5 m, 1 m) and the other is non line-of-sight path at the Rx2 (6 m, 2 m, 1 m). Tx and Rx1 are at a distance of approximately 5.3 meter. Tx and Rx3 are at a distance of approximately 3.2 meter. SBR/Image techniques combined antenna radiation pattern is used to calculate the UWB channel impulse response for each location of the receiver. Channel impulse response of Tx-Rx1 and Tx-Rx2 for UCAA-GA case was shown in Fig. 5(a) and Fig. 5(b) respectively. Channel

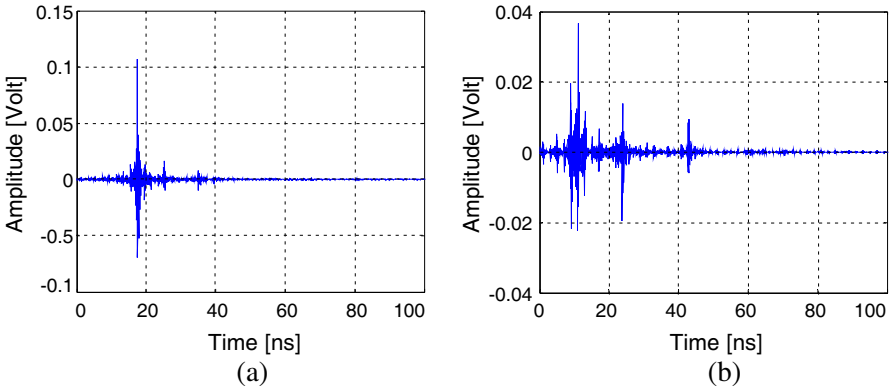


**Figure 5.** The channel impulse response for Scenario I using UCAA-GA of transmitting antennas: (a) Tx-Rx1, (b) Tx-Rx2.

impulse response of Tx-Rx2 was presented in Fig. 5(b). Similar to Fig. 5(a), the transmitting antenna was UCAA-GA. Table 1 shows the RMS delay spread $\tau_{\mathrm{RMS}}$ and mean excess delay spread $\tau_{\mathrm{MED}}$ when using the UCAA-GA to be the transmitting antenna in the Scenario I.

Based on the channel impulse response, the number of multipath components, the RMS delay spread $\tau_{\mathrm{RMS}}$ and the mean excess delay $\tau_{\mathrm{MED}}$ are computed. For Scenario I, the $\tau_{\mathrm{RMS}}$ in Rx1 and Rx2 are 6.13 ns and 8.06 ns, respectively. It is clear that $\tau_{\mathrm{RMS}}$ for the Rx1 is the smaller, since there is a line of sight path for Rx1. The $\tau_{\mathrm{MED}}$ in Rx1 and Rx2 are 2.01 ns and 5.63 ns, respectively. Fig. 6 shows the BER V.S. SNR for Scenario I using three different kinds of transmitters. Here, SNR is defined as the ratio of the average transmitting power to the noise power. The results show that the BER curve decreases greatly when the UCAA-GA is used as transmitter. It is due to the fact that the UCAA-GA can minimize the fading and reduce the mulitpath effects. It also can focus the synthesized antenna array pattern to optimize the available processing gain to the receiver.

**Table 1.** Channel parameters for Rx1 and Rx2 in the Scenario I.

| Channel Parameters \ Receiver Antenna | Rx1 | Rx2 |
|---|---|---|
| $\tau_{\mathrm{MED}}$ (ns) | 2.01 | 5.63 |
| $\tau_{\mathrm{RMS}}$ (ns) | 6.13 | 8.06 |

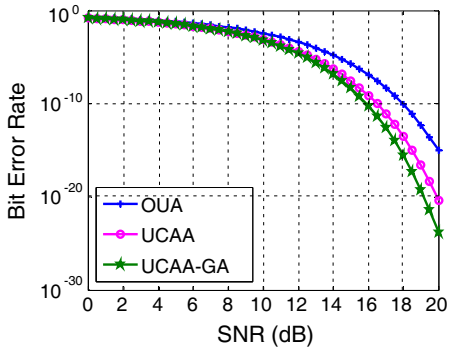


**Figure 6.** BER V.S. SNR over Scenario I for three kinds of transmitters.

Scenario II comprises two receivers: one is non line-of-sight path at the Rx3 (4 m, 2 m, 1 m) and the other is non line-of-sight path at the Rx2. The height of the wooden bookcase was higher than that of the Tx, Rx3 and Rx2. The Tx-Rx3 distance on the horizontal plane is 2 meter in Scenarios II. Channel impulse response of Tx-Rx2 was displayed in Fig. 7(a). In this scenario II, UCAA-GA was used as the transmitting antenna. Channel impulse response of Tx-Rx3 was presented in Fig. 7(b). Similar to Fig. 7(a), the transmitting antenna was UCAA-GA. For Scenario II, the $\tau_{\mathrm{RMS}}$ in Rx3 and Rx2 are 9.87 ns and 11.06 ns respectively. It is clear that $\tau_{\mathrm{RMS}}$ for the Rx3 is the smaller. The $\tau_{\mathrm{MED}}$ in Rx2 and Rx3 are 5.60 ns and 5.49 ns, respectively. Table 2 shows the RMS delay spread $\tau_{\mathrm{RMS}}$ and mean excess delay spread $\tau_{\mathrm{MED}}$ when using the UCAA-GA to be the transmitting antenna in the Scenario II.

Figure 8 shows the BER V.S. SNR for Scenario II, which is non line-of-sight path, using three kinds of transmitters. Fig. 8 also shows the BER V.S. SNR for Scenario II, whose transmitter is UCAA-GA.

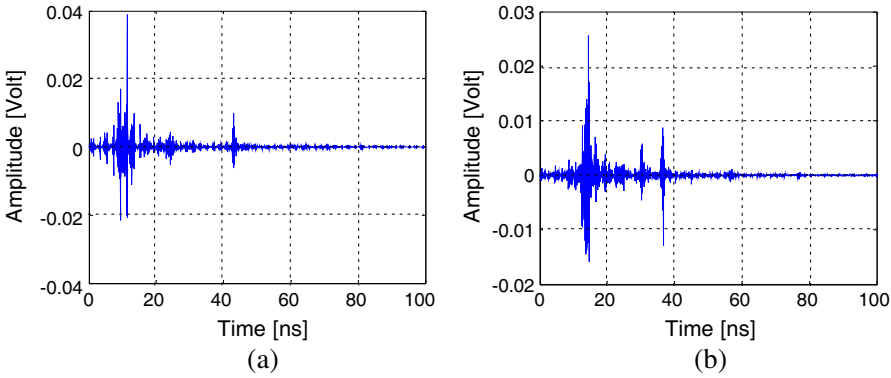


**Figure 7.** The channel impulse response for Scenario II using UCAA-GA of transmitting antennas: (a) Tx-Rx2, (b) Tx-Rx3.

**Table 2.** Channel parameters for Rx2 and Rx3 in the Scenario II.

| Channel Parameters \ Receiver Antenna | Rx2 | Rx3 |
|---|---|---|
| $\tau_{\mathrm{MED}}$ (ns) | 5.60 | 5.49 |
| $\tau_{\mathrm{RMS}}$ (ns) | 11.06 | 9.87 |

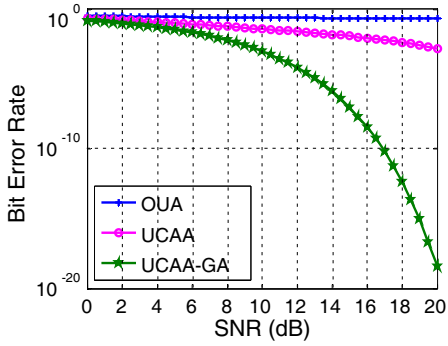


**Figure 8.** BER V.S. SNR over Scenario II for three kinds of transmitters.

The results show that the BER curve decreases a little when using the UCAA-GA as the transmitter.

All of the above results demonstrate the UCAA-GA which presents in this paper is powerful. By applying this antenna array to multiusers propagation environment, it can increase the ratio of combined receiving signal energy to noise. Moreover, there techniques can mitigate severe multipath fading in complex propagation environment. As a result, the BER can be reduced substantially in indoor UWB communication system.

## 5. CONCLUSION

Using the smart UWB circular antenna array to minimize the BER performance in indoor wireless communication is presented. The impulse response of the channel is computed by SBR/Image techniques, inverse fast Fourier transform and Hermitian processing. By using the impulse response of the multipath channel, the BER performance of B-PAM IR UWB communication systems is calculated. In this paper, the fitness function is defined as the reciprocal of BER of the system. The genetic algorithm maximizes the fitness function by adjust the amplitude and feed length of each antenna. Numerical results show that the BER can be reduced substantially in indoor UWB communication system.

## REFERENCES

1. Federal Communications Commission, "Revision of Part 15 of the commission's rules regarding ultra-wideband transmission system,

first report and order," *FCC, ET Docket*, 1–118, Feb. 14, 2002.

2. Colak, S., T. F. Wong, and A. H. Serbest, "UWB dipole array with equally spaced elements of different lengths," *IEEE International Conference on Ultra-wideband*, 789–793, 2007.
3. Malik, W. Q., D. J. Edwards, and C. J. Stevens, "Angular-spectral antenna effects in ultra-wideband communications links," *IEE Proc. — Commun.*, Vol. 153, No. 1, Feb. 2006.
4. Funk, E. E. and C. H. Lee, "Free-space power combining and beam steering of ultra-wideband radiation using an array of laser-triggered antennas," *IEEE Trans. Microwave Theory Tech.*, Vol. 44, 2039–2044, Nov. 1996.
5. Yazdandoost, K. Y. and R. Kohno, "Free-space power combining and beam steering of ultra-wideband radiation using an array of laser-triggered antennas," *IEEE Communication Magazine*, Vol. 42, No. 6, 29–32, 2004.
6. Ghavami, M., "Wideband smart antenna theory using rectangular array structures," *IEEE Trans. Signal Processing*, Vol. 50, No. 9, 2143–2151, Sep. 2002.
7. Tarokh, V., N. Seshadri, and A. R. Calderbank, "Space-time codes for high data rate wireless communications: Performance criterion and code construction," *IEEE Trans. Inform. Theory*, Vol. 44, 744–745, Mar. 1998.
8. Chen, C. H., C. C. Chiu, and C. L. Liu, "Novel directional radiation pattern by genetic algorithms in indoor wireless local loop," *Wireless Personal Communications*, Vol. 42, No. 4, 575–586, Sep. 2007.
9. Ho, M.-H., S.-H. Liao, and C.-C. Chiu, "A novel smart UWB antenna array design by PSO," *Progress In Electromagnetic Research C*, Vol. 15, 103–115, 2010.
10. Ares, F. J., A. Rodriguez, E. Villanueva, and S. R. Rengarajan, "Genetic algorithms in the design and optimization of antenna array patterns," *IEEE Trans. Antennas and Propagat.*, Vol. 47, 506–510, Mar. 1999.
11. Guo, J. L. and J. Y. Li, "Pattern synthesis of conformal array antenna in the presence of platform using differential evolution algorithm," *IEEE Trans. Antennas and Propagation*, Vol. 57, No. 9, 2615–2621, Sep. 2009.
12. Gueguen, E., F. Thudor, and P. Chambelin, "A low cost UWB printed dipole antenna with high performance," *IEEE International Conference on Ultra-wideband*, 89–92, Sep. 2005.
13. Talom, F. T., B. Uguen, L. Rudant, J. Keignart, J.-F. Pintos,

and P. Chambelin, "Evaluation and characterization of an UWB antenna in time and frequency domains," *IEEE International Conference on Ultra-wideband*, 669–673, Sep. 2006.

14. Li, Z. X. and Y. Q. Jin, "Numerical simulation of bistatic scattering from fractal rough surface in the finite element method," *Science in China (Series E)*, Vol. 44, 12–18, 2001.
15. Manteuffel, D., "Radio link characterization using real antenna integration scenarios for UWB consumer electronic applications," *Ultra Wideband Systems, Technologies and Applications*, 123–130, The Institution of Engineering and Technology Seminar, Apr. 2006.
16. El-Hadidy, M. and T. Kaiser, "Impact of ultra wide-band antennas on communications in a spatial cannel," *1st International Cognitive Radio Oriented Wireless Networks and Communications, 2006*, 1–5, Jun. 2006.
17. Malik, W. Q., D. J. Edwards, Y. Zhang, and A. K. Brown, "Three-dimensional equalization of ultrawideband antenna distortion," *Proc. Int. Conf. Electromagn. Adv. Apps. (ICEAA)*, Torino, Italy, Sep. 2007.
18. Yao, R., Z. Chen, and Z. Guo, "An efficient multipath channel model for UWB home networking," *2004 IEEE Radio and Wireless Conference*, 511–516, Sep. 2004.
19. Oppermann, I., M. Hamalainen, and J. Iinatti, *UWB Theory and Applications*, John Wiley & Sons, 2004.
20. Liu, C. L., C. C. Chiu, S. H. Liao, and Y. S. Chen, "Impact of metallic furniture on UWB channel statistical characteristics," *Tamkang Journal of Science and Engineering*, Vol. 12, No. 3, 271–278, Sep. 2009.
21. Goldberg, D. E., *Genetic Algorithm in Search, Optimization and Machine Learning*, Addison Wesley, 1989.
22. Michael Johnson, J. and Y. Rahmat-Samii, "Genetic algorithms in engineering electromagnetics," *IEEE Antennas and Propagation Magazine*, Vol. 39, No. 4, 7–21, Aug. 1997.